Geology
August 2019, Volume 47 Issue 8 Pages 762-766
https://doi.org/10.1130/G46047.1
https://archimer.ifremer.fr/doc/00593/70506/

Archimer
https://archimer.ifremer.fr

Critical role of caldera collapse in the formation of seafloor mineralization: The case of Brothers volcano

De Ronde Cornel E. J. [1], Humphris Susan E. [2], Hofig Tobias W. [3], Reyes Agnes G. [1], The Iodp Expedition 376 Scientists

[1] GNS Sci, 1 Fairway Dr, Lower Hutt 5040, New Zealand.
[2] Woods Hole Oceanog Inst, Dept Geol & Geophys, Woods Hole, MA 02543 USA.
[3] Texas A&M Univ, Int Ocean Discovery Program, 1000 Discovery Dr, College Stn, TX 77845 USA.

Abstract :

Hydrothermal systems hosted by submarine arc volcanoes commonly include a large component of magmatic fluid. The high Cu-Au contents and strongly acidic fluids in these systems are similar to those that formed in the shallow parts of some porphyry copper and epithermal gold deposits mined today on land. Two main types of hydrothermal systems occur along the submarine portion of the Kermadec arc (offshore New Zealand): magmatically influenced and seawater-dominated systems. Brothers volcano hosts both types. Here, we report results from a series of drill holes cored by the International Ocean Discovery Program into these two types of hydrothermal systems. We show that the extent of hydrothermal alteration of the host dacitic volcaniclastics and lavas reflects primary lithological porosity and contrasting spatial and temporal contributions of magmatic fluid, hydrothermal fluid, and seawater. We present a two-step model that links the changes in hydrothermal fluid regime to the evolution of the volcano caldera. Initial hydrothermal activity, prior to caldera formation, was dominated by magmatic gases and hypersaline brines. The former mixed with seawater as they ascended toward the seafloor, and the latter remained sequestered in the subsurface. Following caldera collapse, seawater infiltrated the volcano through fault-controlled permeability, interacted with wall rock and the segregated brines, and transported associated metals toward the seafloor and formed Cu-Zn-Au-rich chimneys on the caldera walls and rim, a process continuing to the present day. This two-step process may be common in submarine arc caldera volcanoes that host volcanogenic massive sulfide deposits, and it is particularly efficient at focusing mineralization at, or near, the seafloor.

Please note that this is an author-produced PDF of an article accepted for publication following peer review. The definitive publisher-authenticated version is available on the publisher Web site.

INTRODUCTION

Volcanogenic massive sulfide (VMS) deposits are a significant source of metals (largely Cu, Zn, Pb ± Au) critical for modern society, thus understanding their genesis remains a key part of any exploration strategy. The geological record has several examples where sizeable VMS deposits appear to have formed within submarine arc

caldera volcanoes (e.g. Large et al., 2001), including some that appear to be the shallow expression of porphyry Cu deposits (Sillitoe et al., 1996; Hedenquist et al., 2018).

The Kermadec arc, offshore New Zealand, is host to 34 large volcanic complexes, of which 26 are hydrothermally active (de Ronde et al., 2001, 2003). Brothers submarine volcano was selected by the international science community as an ideal place to drill into a caldera to provide the missing link (i.e., the 3rd dimension) in our understanding of mineral deposit formation along arcs, the subseafloor architecture of these volcanoes, and their related permeability (de Ronde et al., 2017).

BROTHERS VOLCANO AND ITS HYDROTHERMAL SYSTEMS

Brothers volcano rises from a depth of ~2,200 m to a continuous caldera rim at 1,540 m, shoaling to 1,320 m at its northwestern rim (Fig. 1). The 3–3.5 km diameter caldera floor is surrounded by 290–530 m high walls and contains an elongate NE-SW, 1.5–2 km wide and 350 m high, post-collapse cone (Upper Cone) that shoals to 1,220 m; a smaller satellite cone (Lower Cone) overlaps its NE flank (Fig. 1) (de Ronde et al., 2005; Embley et al., 2012).

Brothers volcano hosts two active but very distinct types of hydrothermal systems (de Ronde et al., 2005, 2011). The first type is dominated by seawater-rock reactions and includes the active vent fields of the Upper Caldera, NW Caldera and W Caldera, and the inactive SE Caldera site (Fig. 1). This type is characterized by high-temperature (≤320°C), moderately acidic (pH = 3.2) fluids that contain modest gas abundances (CO_2 =

13–40 mM), and Cu-Zn-Au-rich sulfide chimneys. By contrast, the second type is strongly influenced by magmatic fluids (largely gases) and includes the hydrothermal systems at the Upper and Lower Cones (Fig. 1). This type is characterized by lower-temperature (≤120°C), very low pH (to 1.9), gas-rich (CO_2 = ≤206 mM) fluids, with native sulfur chimneys and extensive Fe-oxyhydroxide crusts (de Ronde et al., 2011). Vent fluid $^3He/^4He$ values suggest that the heat driving both types is derived from the same underlying magma source, with fluids discharged from the Cone sites following a more direct pathway than those beneath the NW Caldera site (de Ronde et al., 2011).

SAMPLING AND METHODS

International Ocean Discovery Program (IODP) Expedition 376 drilled five sites on Brothers volcano between May and July 2018, recovering 222.4 m of core that consists largely of dacitic volcaniclastics (breccia) and lava flows. Alteration is pervasive and mineral assemblages are complex and variable, attesting to multifaceted and changeable hydrothermal systems. Here we focus on the three longest holes; Hole U1527C that cored 238 m below the NW Caldera rim on the western margin of the NW Caldera vent field; Hole U1530A that cored 453 m from immediately above an exposed stockwork zone in the central part of the NW Caldera vent field with active chimneys nearby, to near the bottom of the caldera; and Hole U1528D that cored 359 m through the Upper Cone from the floor of a ~25 m diameter pit crater (Fig. 1; de Ronde et al., 2019a).

All analyses were conducted onboard the D/V *JOIDES Resolution*. Polished thin

sections were observed under both transmitted and reflected light using a polarizing microscope equipped with a digital camera for microphotography. X-ray diffraction data were generated by a Bruker D4Endeavor X-ray diffractometer using a generator voltage of 35 kV and current of 40 mA, and were evaluated against the International Center for Diffraction Data database for minerals using the Search/Match component of Bruker's EVA Diffraction Evaluation software.

Borehole fluids were analyzed by ICP-AES and gas chromatography following standard shipboard procedures described in Murray et al. (2000).

Fluid inclusions were measured using a USGS-adapted FLUID INC. heating/freezing stage. Wherever possible, inclusions from drusy crystals of translucent anhydrite, quartz, natroalunite or gypsum protruding into partially open vugs and fractures and/or in cross-cutting veins were analyzed in order to determine the present or most recent fluid temperatures and salinities involved in rock alteration (further details and images are available in the Data Repository).

RESULTS AND DISCUSSION

Hydrothermal Alteration Mineral Assemblages

Cores recovered from the NW Caldera hydrothermal field show alteration under three different conditions. The upper parts of Hole U1527C (to 185 meters below seafloor [mbsf]) and Hole U1530A (to 30 mbsf; Fig. 1) are characterized by a secondary mineral assemblage of goethite + opal CT + zeolites resulting from low-temperature (<150°C;

Steiner, 1953) reaction of rock with seawater. In Hole U1527C, this is underlain by a higher-temperature (≤ 250°C; Hemley et al., 1980) alteration assemblage dominated by chlorite + quartz + illite + pyrite (de Ronde et al., 2019a). In Hole U1530A, the low-temperature assemblage is underlain by a similar green-gray alteration assemblage of quartz + illite + chlorite ± anhydrite ± pyrite ± sphalerite ± smectite. Notably, a deeper alteration assemblage of diaspore + quartz + pyrophyllite ± rutile ± zunyite was identified in the lower part of Hole U1530A (from ~225 mbsf; Fig. 2; de Ronde et al., 2019b)—indicative of still higher temperatures (i.e., 230–350°C)—which formed through reaction of rocks with acid-sulfate fluids (Reyes, 1990; Stoffregen et al., 2000). In the deepest parts of Hole U1530A, these diaspore and/or pyrophyllite zones are intercalated and locally overprinted by chlorite and illite-bearing assemblages, indicative of reaction with a relatively high-temperature, seawater-dominated fluid.

Temperature profiles in Hole 1530A are concave with temperatures gradually increasing downhole, consistent with seawater recharge occurring in the system (de Ronde et al., 2019b). In addition, a rapid decrease of temperature (from 94°C to 37°C) with time was observed near the bottom of the hole after drilling was stopped. When combined with overprinting chlorite + illite and oxidized surfaces on almost all of the open fractures, this indicates permeable flow zones and the incursion of heated seawater since the formation of the higher-temperature diaspore/ pyrophyllite zones.

By contrast, the breccia and dacitic lavas recovered from the Upper Cone (Hole U1528D) have three different, often intercalated alteration assemblages, all of which

include variable proportions of illite, natroalunite, pyrophyllite, quartz, opal-CT, pyrite and native sulfur, as well as other accessory minerals like rutile (de Ronde et al., 2019c). As is the case near the bottom of Hole U1530A, these mineral assemblages also attest to high-temperature (230–350°C) reaction of rocks with acid-sulfate fluids that can be derived from the disproportionation of magmatic sulfur gases (e.g., SO_2 and H_2S) (Giggenbach, 1997), with the presence of native sulfur clearly indicating a magmatic input (Giggenbach, 1996; Christenson et al., 2010). The intensely altered rocks present in Hole U1528D exhibit extreme depletion of major cation oxides, such as MgO, K_2O, CaO, MnO and Na_2O (for more information, see the Data Repository and de Ronde et al., 2019c).

Borehole Fluid Compositions

Three borehole fluid samples were collected from Hole U1528D at depths of ~160, ~279 and ~313 mbsf. Temperatures of 140°C, 212°C and >236°C for the samples, respectively, were determined by downhole logging. The fluids have nearly identical Ca, Br, and Mg contents, and are depleted in Na by 30-37% and in Cl by 12-16% relative to seawater (Fig. 3). They are gas-rich with high ΣH_2S concentrations (14.6 mM), highly elevated ΣSO_4 contents (≤88.9 mM) and are very acidic (pH ≥1.8), characteristic of acid-sulfate fluids (for more information, see de Ronde et al., 2019c).

Fluid Inclusion Data

141 Fluid inclusion data derived from anhydrite, quartz and natroalunite crystals from both
142 the Cone and NW Caldera boreholes fall into two distinct groups (Fig. 3); one population
143 with lesser-than and up-to-3 times higher than seawater (3.2 wt.% NaCl equiv.) salinities,
144 similar to the borehole fluids, and hypersaline brines (~32-45 wt.% NaCl equiv.; see Data
145 Repository and de Ronde et al., 2019a, for further information). Curves have been
146 calculated (Bischoff and Pitzer, 1989; Driesner and Heinrich, 2007) then plotted in Figure
147 3, with the goal of describing formation mechanisms for the fluids trapped by the
148 inclusions. Trajectory A derives from possible higher-temperature supercritical fluid
149 condensation through cooling. Three other trajectories were calculated assuming phase-
150 separation of heated seawater via depressurization at 380°C (255 bar; trajectory B) and
151 400°C (281 bar; trajectory C), respectively, and 415°C (321 bar; trajectory D) for a 4.2
152 wt.% NaCl equivalent fluid that represents the best fit for the most recent two-phase fluid
153 inclusions seen the Cone site samples (Fig. 3). Hypersaline liquid condensed from the
154 magmatic-hydrothermal interface is given by trajectory E to best explain the presence of
155 hypersaline aqueous fluids in inclusions that include a vapor bubble, sulfur, and daughter
156 minerals of sulfides and salts (see Data Repository). Isobaric phase separation (trajectory
157 F) may cause a slight decrease in salinity within a narrow range of temperatures for the
158 brine inclusions. These trajectories suggest that subcritical phase separation of seawater
159 cannot produce the NW Caldera fluid inclusion compositions of >5 wt.% NaCl, nor the
160 hypersaline brines. Rather, we suggest that inclusions with salinities >5 wt.% NaCl
161 equivalent are derived from a fluid condensed from the supercritical region followed by

phase separation (trajectory D), whereas the hypersaline brine originated from either condensation of a single-phase fluid at higher temperatures and pressures at the magmatic-hydrothermal interface (Gruen et al., 2014), or exsolution from a silicate melt (Heinrich, 2007).

LINKING HYDROTHERMALSM TO THE EVOLUTION OF BROTHERS VOLCANO

The downhole record of hydrothermal alteration at Brothers volcano revealed by drilling suggests a progression from an initially magmatically-influenced to a seawater-dominated hydrothermal system. A conceptual model (Fig. 4) links the changes in hydrothermal fluid regime to the evolution of the volcano caldera and explains how magmatic-hydrothermal systems can ultimately produce Cu-Au-rich VMS deposits. In the pre-caldera stage, the volcano hosts a hydrothermal system dominated by magmatic volatiles and metal-rich brines (Fig. 4A). Eruption conditions at Brothers (e.g., magma volatile contents, hydrostatic pressure at vent depth) combine to produce abundant volcaniclastics, including ubiquitous breccia. When combined with 'damage zones' created as a result of large, post-eruption pressure transients (Cole et al., 2005), these key conditions strongly influence primary porosity, providing first-order control on alteration zonation. Initial expulsion of magmatic heat and volatiles is manifest by low-salinity, vapor-rich, metal-poor fluids, while magmatically-derived metal-rich brines are segregated and temporarily trapped within the breccia (Gruen et al., 2014; Weis, 2015). This is consistent with modeling experiments for porphyry Cu deposits that show

marginal near-vertical and carapace sub-horizontal alteration zones derive from hydrothermal fluids (Weis et al., 2012), similar to those depicted in Fig. 4. Caldera collapse then occurred after a singularly large, or series of volcanic eruptions, that deposited 185 m of the relatively fresh volcaniclastics intersected in Hole U1527C (Fig. 4B). Post-collapse, a resurgent cone developed and hosted a new, magmatically-influenced hydrothermal system (Fig. 4C). Simultaneously, ingress of seawater occurred down faults marking the caldera wall (not shown) and along the base of the caldera, and reacted with the rocks and trapped brines, transporting the metals to the seafloor to form present-day Cu-Zn-Au-rich chimneys (Fig. 4C). We conclude that the preponderance of caldera volcanoes as hosts to intraoceanic arc VMS mineralization reflects a two-step process for their formation. Ancient arc-related VMS deposits in the geological record likely also formed via a similar mechanism.

ACKNOWLEDGMENTS

This research used samples and data provided by IODP. We sincerely thank the IODP technical staff and the D/V *JOIDES Resolution* crew for their invaluable support, determination, and perseverance during what was a challenging expedition. We gratefully acknowledge S.L. Walker for compiling the base bathymetry in Fig. 1, H.A. Berkenbosch for helping to construct Fig. 4 and C.J.N. Wilson for discussion. The manuscript benefited from helpful reviews by three anonymous reviewers.

REFERENCES CITED

Bischoff, J.L. and Rosenbauer, R.J., 1985, An empirical equation of state for hydrothermal seawater (3.2 percent NaCl): Am. J. Sci., v. 285, p, 725-763.

Bischoff, J.L. and Pitzer, K.S., 1989, Liquid vapor relations for the system NaCl-H_2O: summary of the P-T-x surface from 300º to 500ºC: Am. J. Sci. v. 289, 217-248.

Caratori Tontini, F., Davy, B., de Ronde, C.E.J., Embley, R.W., Leybourne, M.I. and Tivey, M.A., 2012, Crustal magnetization of Brothers volcano, New Zealand, measured by autonomous underwater vehicles: geophysical expression of a submarine hydrothermal system: Econ. Geol., v. 107, p. 1571-1581.

Christenson, B.W., Reyes, A.G., Young, R., Moebis, A., Sherburn, S., Cole-Baker, J. and Britten, K., 2010, Cyclic processes and factors leading to phreatic eruption events: Insights from the 25 September 2007 eruption through Ruapehu Crater Lake, New Zealand: J. Volcanol. Geothermal Res., v. 191, p. 15–32.

Cole, J.W., Milner, D.M. and Spinks, K.D., 2005, Calderas and caldera structures: a review: Earth Science Reviews, v. 69, p. 1-26.

de Ronde, C.E.J., Baker, E.T., Massoth, G.J., Lupton, J.E., Wright, I.C., Feely, R.A. and Greene, R.R., 2001, Intra-oceanic subduction-related hydrothermal venting, Kermadec volcanic arc, New Zealand: Earth Planet. Sci. Lett., v. 193, p. 359-369.

de Ronde, C.E.J., Massoth, G.J., Baker, E.T. and Lupton, J.E. , 2003, Submarine hydrothermal venting related to volcanic arcs, *in* Simmons, S.F. and Graham, I.G. eds., Giggenbach Memorial volume, Soc. Econ. Geol. and Geochem. Soc. Special

Publ., v. 10, p. 91-109.

de Ronde, C.E.J, Hannington, M.F., Stoffers, P., Wright, I.C., Ditchburn, R.G., Reyes, A.G., Baker, E.T., Massoth, G.J., Lupton, J.E., Walker, S.L., Breene, B.R., Soong, C.W., Ishibashi, J., Lebon, G.T., Bray, C.J.. and Resing, J.A., 2005, Evolution of a submarine magmatic-hydrothermal system: Brothers volcano, southern Kermadec arc, New Zealand: Econ. Geol., v. 100, p. 1097-1133.

de Ronde, C.E.J., Massoth, G.J., Butterfield, D.A., Christenson, B.W., Ishibashi, J., Ditchburn, R.G., Hannington, M.D., Brathwaite, R.L., Lupton, J.E., Kamenetsky, V.S., Graham, I.J., Zellmer, G.F., Dziak, R.P., Embley, R.W., Dekov, V.M., Munnik, F., Lahr, J., Evans, L.J., and Takai, K., 2011, Submarine hydrothermal activity and gold-rich mineralization at Brothers volcano, Kermadec arc, New Zealand: Mineralium Deposita, v. 46, p. 541-584, 2011.

de Ronde, C.E.J., Humphris, S.E. and Höfig, T.W., 2017, Expedition 376 Scientific Prospectus: Brothers Arc Flux. International Ocean Discovery Program. https://doi.org/10.14379/iodp.sp.376.2017, 33 pp.

de Ronde, C.E.J., Humphris, S.E., Höfig, T.W. and the Expedition 376 Scientists, 2019a, *Brothers Arc Flux*. Proceedings of the International Ocean Discovery Program, 376: College Station, TX (International Ocean Discovery Program). https://doi.org/10.14379/iodp.proc.376.2019 , in press.

de Ronde, C.E.J., Humphris, S.E., Höfig, T.W. and the Expedition 376 Scientists, 2019b, Site U1530. *In,* de Ronde, C.E.J., Humphris, S.E., Höfig, T.W., and the Expedition

376 Scientists, *Brothers Arc Flux*. Proceedings of the International Ocean Discovery Program, 376: College Station, TX (International Ocean Discovery Program). https://doi.org/10.14379/iodp.proc.376.106.2019 , in press.

de Ronde, C.E.J., Humphris, S.E., Höfig, T.W., and the Expedition 376 Scientists, 2019c, Site U1528. *In,* de Ronde, C.E.J., Humphris, S.E., Höfig, T.W., and the Expedition 376 Scientists, *Brothers Arc Flux*. Proceedings of the International Ocean Discovery Program, 376: College Station, TX (International Ocean Discovery Program). https://doi.org/10.14379/iodp.proc.376.104.2019 , in press.

Driesner, T. and Heinrich, C.A., 2007. The system H_2O–NaCl. Part I: Correlation formulae for phase relations in temperature–pressure–composition space from 0 to 1000 C, 0 to 5000 bar, and 0 to 1 X_{NaCl}: Geochim. Cosmochim. Acta, v. 71, p, 4880-4901.

Embley, R.W., de Ronde, C.E.J., Merle, S.G., Davy, B. and Caratori Tontini, F. 2012, Detailed morphology and structure of an active submarine arc caldera: Brothers volcano, Kermadec arc: Econ. Geol., v. 107, p. 1557-1570.

Giggenbach, W.F. 1996, Chemical composition of volcanic gases, *in*, Scarpa, R. and Tilling, R.I., eds,, Monitoring and Mitigation of Volcano Hazards, Springer, p. 221–256.

Giggenbach, W.F, 1997, The origin and evolution of fluids in magmatic-hydrothermal systems, *in* Barnes, H.L., ed,. Geochemistry of Hydrothermal Ore Deposits. 2nd Edition, John Wiley & Sons, Inc., p. 737-796.

267 Gruen, G., Weis, P., Driesner, T., Heinrich, C.A. and de Ronde, C.E.J., 2014,
268 Hydrodynamic modeling of magmatic-hydrothermal activity at submarine arc
269 volcanoes, with implications for ore formation: Earth Planet. Sci. Lett, v. 404, p.
270 307-318.
271 Hedenquist, J.W., Taguchi, S. and Shinohara, H., 2018, Features of large magmatic–
272 hydrothermal systems in Japan: Characteristics similar to the tops of porphyry copper
273 deposits: Resource Geol., v. 60, p. 164-180.
274 Heinrich C.A., 2007, Fluid-fluid interactions in magmatic-hydrothermal ore formation:
275 Reviews in Mineralogy and Geochemistry, v. 65, p. 363-387, Geol. Soc. America.
276 Hemley, J.J., Montoya, J.W., Marinenko, J.W. and Luce, R.W., 1980, Equilibria in the
277 system Al_2O_3-SiO_2-H_2O and some general implications for alteration-mineralization
278 processes: Econ. Geol., v. 75, p. 210–228.
279 Henley, R.W., Truesdell, A.H, Barton, P,B. and Whitney, J.A., 1984, Fluid-mineral
280 equilibria in hydrothermal systems. Reviews in Econ. Geol, vol. 1, Society of
281 Economic Geologists, Texas, 267 pp.
282 Large, R.R., Allen, R.L., Blake, M.D. and Herrmann, W., 2001, Hydrothermal alteration
283 and volatile element halos for the Rosebery K lens volcanic-hosted massive sulfide
284 deposit, western Tasmania: Econ. Geol., v. 96, p. 1055-1072 .
285 Murray, R.W., Miller, D.J., and Kryc, K.A., 2000, Analysis of major and trace elements
286 in rocks, sediments, and interstitial waters by inductively coupled plasma–atomic

emission spectrometry (ICP-AES). Ocean Drilling Program Technical Note, 29. http://dx.doi.org/10.2973/odp.tn.29.2000.

Reyes, A.G., 1990, Petrology of Philippine geothermal systems and the application of alteration mineralogy in their assessment: Volcanol. Geotherm. Res., v. 43, p. 279-309.

Sillitoe, R.H., Hannington, M.D. and Thompson, J.F., 1996, High sulfidation deposits in the volcanogenic massive sulfide environment: Econ. Geol., v. 91, p. 204-212.

Steiner, A., 1953, Hydrothermal rock alteration at Wairakei, New Zealand: Econ. Geol., v. 48, p. 1-13.

Stoffregen, R.E., Alpers, C.N. and Jambor, J.L., 2000, Alunite-jarosite crystallography, thermodynamics, and geochronology, *in* Alpers, C.N., Jambor, J.L. and Nordstrom, D.K., eds., Reviews in Mineralogy and Geochemistry, v. 40, p. 453–479, Geol. Soc. America.

Tanger, J.C. and Pitzer, K.S., 1989, Thermodynamics of NaCl-H_2O: a new equation of state for the near-critical region and comparison with other equations for adjoining regions: Geochim. Cosmochim. Acta, v. 53, p. 973-987.

Weis, P., 2015, The dynamic interplay between saline fluid flow and rock permeability in magmatic-hydrothermal systems: Geofluids, v. 15, p. 350–371.

Weis, P., Driesner, T. and Heinrich, C.A., 2012, Porphyry-copper ore shells form at stable pressure-temperature fronts within dynamic fluid plumes: Science. v. 338, p. 1613-1616.

FIGURE CAPTIONS

Figure 1. Map showing high-resolution (2 m) Autonomous Underwater Vehicle (AUV)-derived bathymetry of Brothers volcano caldera walls and resurgent cones overlain on 25 m resolution ship-derived bathymetry for the caldera floor, upper caldera rim, and volcano flanks. The translucent areas depict zones of low magnetization intensity associated with hydrothermal fluid upflow zones (Caratori Tontini et al., 2012) and incorporate the known vent fields (with the exception of the Lower Cone), including: Upper Caldera; NW Caldera; W Caldera; SE Caldera (extinct) and Upper Cone. IODP Holes U1527C, U1528D and U1530A are the boreholes referred to in the text. The section shown in Fig. 4 is the same as the seismic section shown in de Ronde et al. (2017) for seismic line Bro-3, with Holes U1527C and U1530A projected onto the line. Transverse mercator projection, central meridian = 179°E.

Figure 2. Downhole distribution of primary (plagioclase and cristobalite) and alteration (others) minerals from Hole U1530A. Mineral abundances are semi-quantitative, and were determined by shipboard XRD analysis. Colors refer to different alteration types that are based on characteristic alteration mineral assemblages (see text). H_2S odour (given by the yellow labels embedded in the Igneous unit column) was detected on a number of occasions throughout the drill hole. The different igneous units 1-5 are described in de Ronde et al. (2019b).

Figure 3. Fluid inclusion salinity (expressed as NaCl wt. % equiv.) vs. homogenization

329 temperatures and corresponding enthalpy of NaCl-H_2O (Bischoff and Rosenbauer, 1985;
330 Tanger and Pitzer, 1989). Borehole fluid salinity is plotted at logged temperatures. The
331 plot is divided into subcritical and supercritical regions by the critical line (dashed) with
332 phase separation equations and fluid properties, and critical and halite liquidus curves
333 calculated from Driesner and Heinrich (2007 and references therein) and boiling curve
334 equations adapted from Henley et al. (1984). Bold dashed line demarcates seawater
335 salinity of 3.2 wt. % NaCl equivalent. Phase separation within the subcritical regions
336 consists of; (A) vapor condensation through cooling, (B-D) boiling, or flashing (i.e.,
337 vapor loss) with depressurization, (E) three-phase condensation of liquid, vapor and solid
338 (halite) and (F) isobaric phase separation—see text.
339 **Figure 4**. Schematic depicting the evolution of the caldera and hydrothermal system at
340 Brothers volcano. A. Thermal model depicting isotherms (in °C) for the initial
341 stratovolcano that was host to a magmatic-hydrothermal system dominated by magmatic
342 gases (pink arrows), which likely breached the seafloor, later mantled by volcanic
343 material from a single large, or series of eruptions, that was followed by caldera collapse.
344 Cross hatching denotes brines and/or magmatic salt. B. Main-stage caldera collapse.
345 Schematic shows alteration model (zonation) that is compressed and/or truncated
346 adjacent to the caldera walls. Red triangles represent a dismembered dike; long black
347 dashes, the base of the caldera (de Ronde et al., 2017). C. Thermal model for the post-
348 collapse, resurgent cone (Upper Cone) as it progressively built up from the caldera floor
349 (smaller dashes), itself host to a magmatic-hydrothermal system. Heat from the magma

supplying the Cone also drives seawater circulation through faults along the caldera wall. Blue arrows depict the recharge of seawater in the system, utilizing faults marking the caldera walls (not shown) and higher porosity zones in the caldera floor and Cone. Red arrows denote heated (modified) seawater after it has interacted and/or exchanged with previously deposited metal-rich brines, transporting Cu-Zn-Au mineralization to the seafloor. Scale 1:1. Images shown are representative of alteration assemblages found within an individual borehole (de Ronde et al., 2019a). Mineral abbreviations given in the legends relate to the dominant and/or presence of a diagnostic mineral for a particular alteration zone: an, anhydrite; ba, barite; chl, chlorite; dia, diaspore; goe, goethite; ill, illite; mor, mordenite; natro, natroalunite; op, opal-CT; py, pyrite; pyr, pyrophylllite; qtz, quartz; sul, sulfur; sm, smectite; sph, sphalerite; rut, rutile; zun, zunyite.

[1]GSA Data Repository item 201Xxxx, which consists of a list of the IODP Expedition 376 Scientists, details of methods and equipment used to determine alteration mineral paragenesis and geochemical analysis, methods and images of fluid inclusions analysis, and an explanation of the data and methods used in construction of the model presented in the paper, is available online at www.geosociety.org/pubs/ft20XX.htm, or on request from editing@geosociety.org or Documents Secretary, GSA, P.O. Box 9140, Boulder, CO 80301, USA.

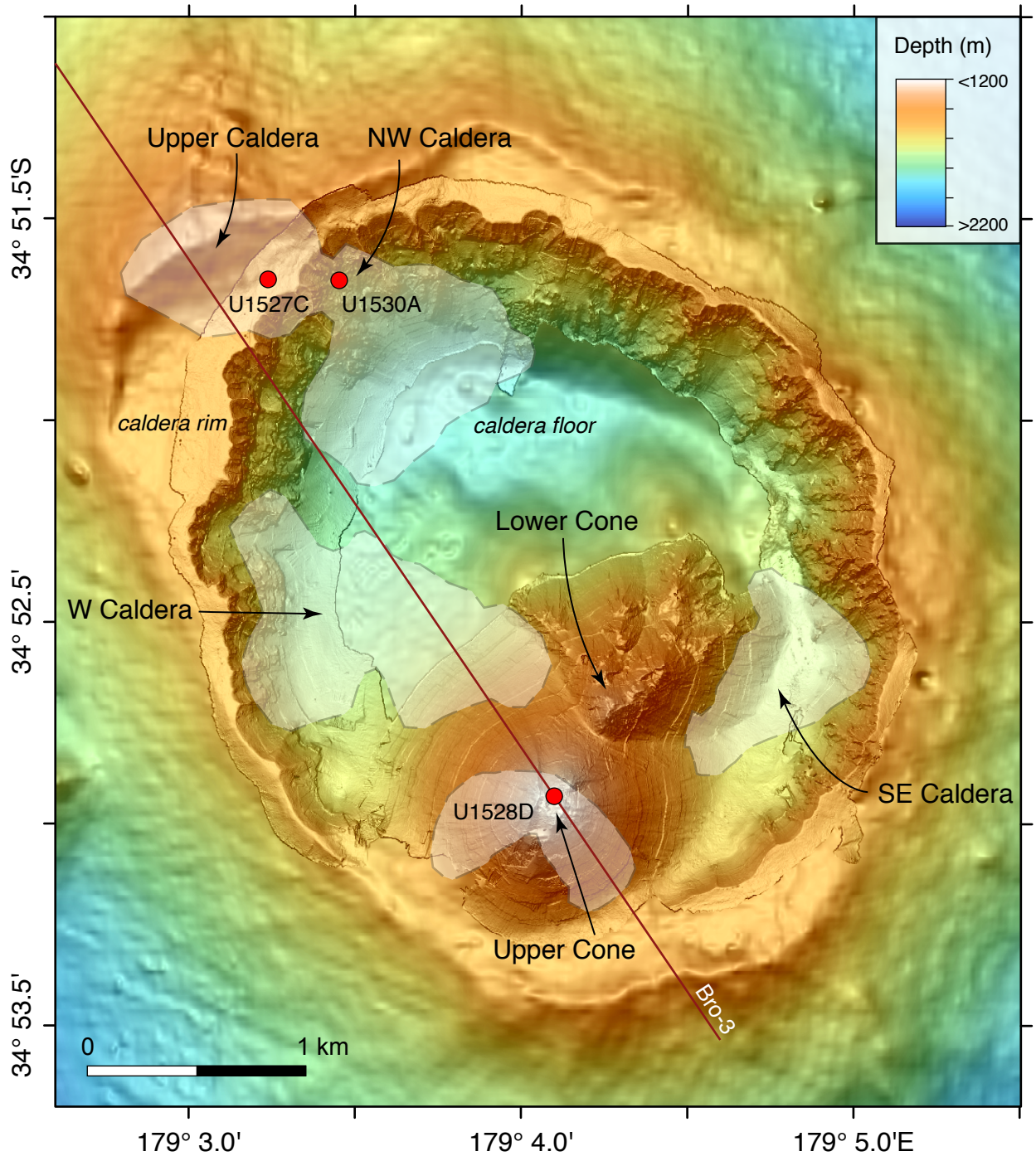
Depth (m)
<1200
>2200
Upper Caldera
NW Caldera
U1527C
U1530A
caldera rim
caldera floor
Lower Cone
W Caldera
SE Caldera
U1528D
Upper Cone
Bro-3
0
1 km
34° 51.5'S
34° 52.5'
34° 53.5'
179° 3.0'
179° 4.0'
179° 5.0'E

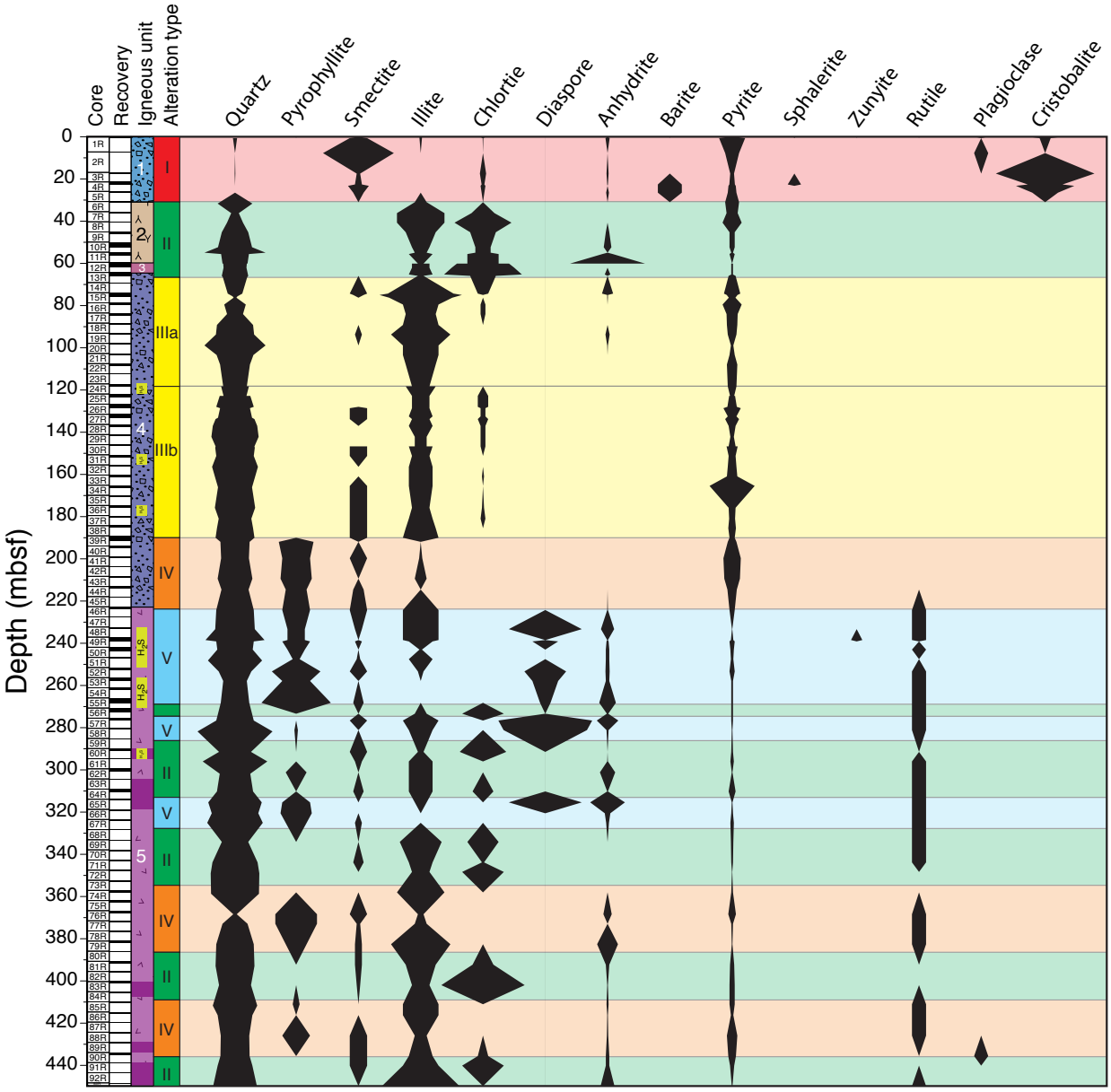
Core
Recovery
Igneous unit
Alteration type
Quartz
Pyrophyllite
Smectite
Illite
Chlortie
Diaspore
Anhydrite
Barite
Pyrite
Sphalerite
Zunyite
Rutile
Plagioclase
Cristobalite
Depth (mbsf)
0
20
40
60
80
100
120
140
160
180
200
220
240
260
280
300
320
340
360
380
400
420
440
I
II
IIIa
IIIb
IV
V
V
II
V
II
IV
II
IV
II
1
2
3
4
5
H2S
H2S

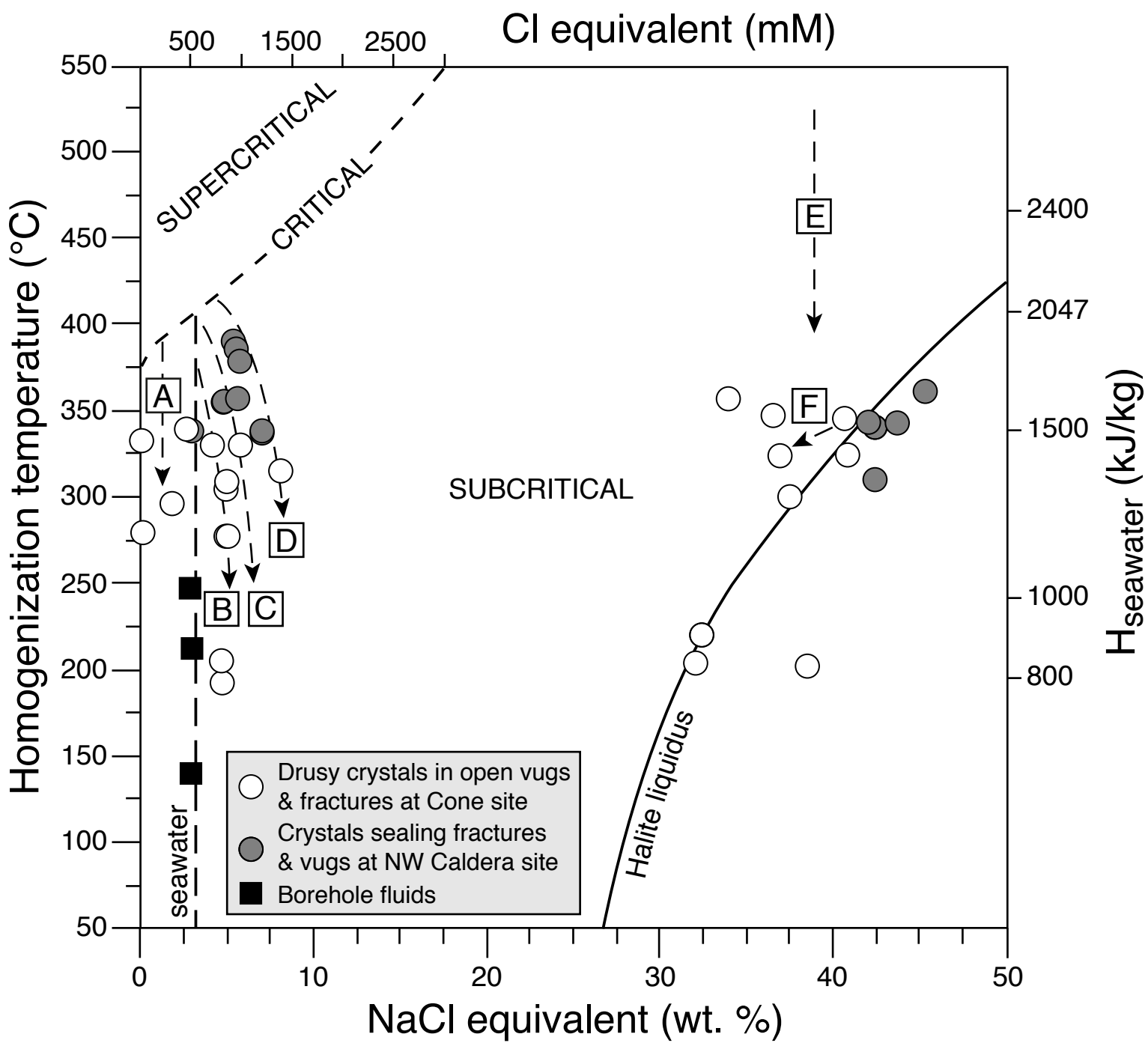
Cl equivalent (mM)
500
1500
2500
550
500
450
400
350
300
250
200
150
100
50
SUPERCRITICAL
CRITICAL
SUBCRITICAL
A
B
C
D
E
F
seawater
Halite liquidus
Drusy crystals in open vugs & fractures at Cone site
Crystals sealing fractures & vugs at NW Caldera site
Borehole fluids
Homogenization temperature (°C)
2400
2047
1500
1000
800
Hseawater (kJ/kg)
0
10
20
30
40
50
NaCl equivalent (wt. %)

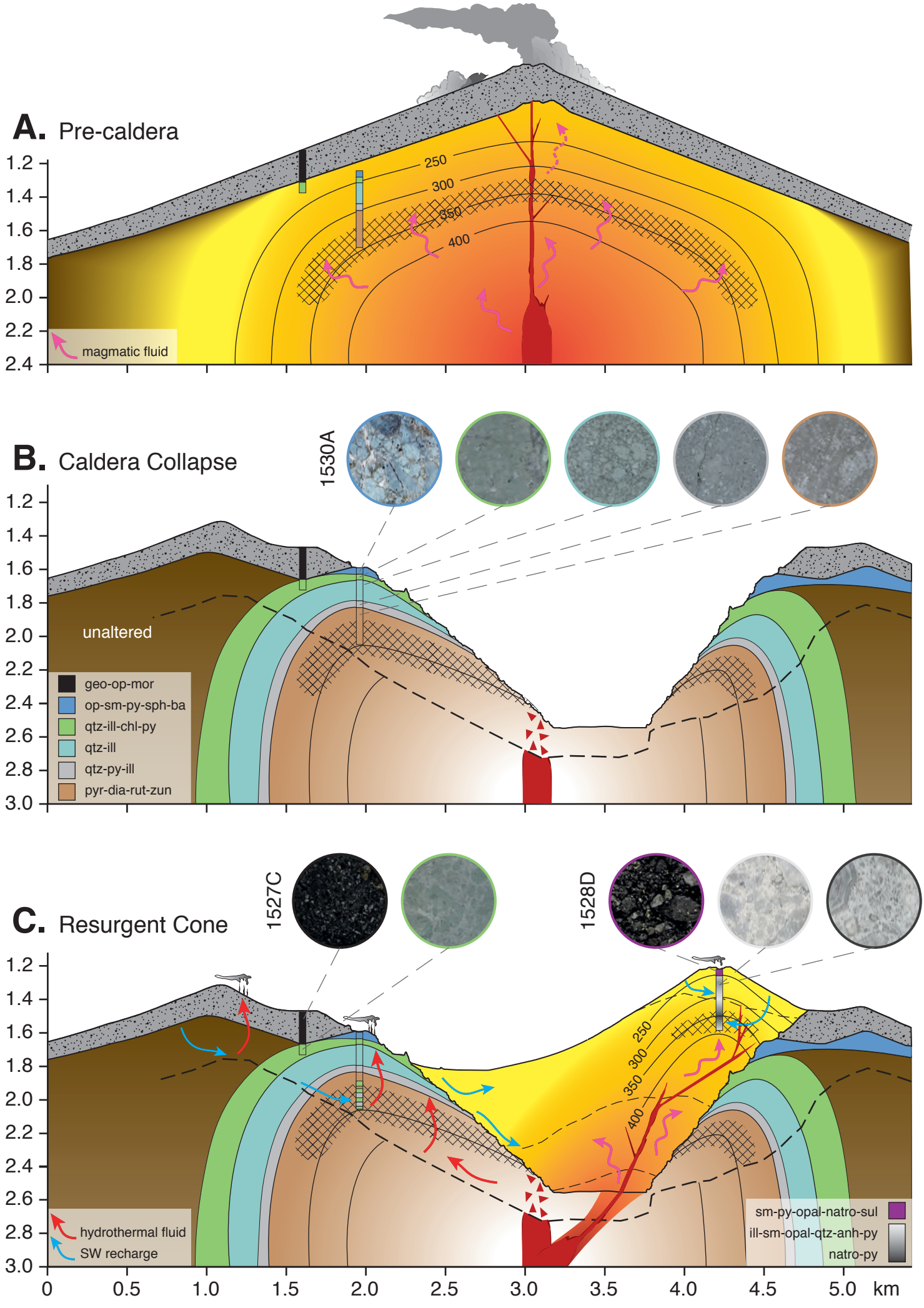
A. Pre-caldera
250
300
350
400
magmatic fluid
B. Caldera Collapse
1530A
unaltered
geo-op-mor
op-sm-py-sph-ba
qtz-ill-chl-py
qtz-ill
qtz-py-ill
pyr-dia-rut-zun
C. Resurgent Cone
1527C
1528D
hydrothermal fluid
SW recharge
sm-py-opal-natro-sul
ill-sm-opal-qtz-anh-py
natro-py
1.2
1.4
1.6
1.8
2.0
2.2
2.4
2.6
2.8
3.0
0
0.5
1.0
1.5
2.0
2.5
3.0
3.5
4.0
4.5
5.0
km